

Changes to the ^{252}Cf neutron spectrum caused by source encapsulation

R. Weinmann-Smith^{1,2}, S. Croft³, M.T. Swinhoe¹, A. Enqvist²

¹ Safeguards Science and Technology Group (NEN-1), Nuclear Nonproliferation Division, Los Alamos National Laboratory, NM 87545, USA
E-mail: swinhoe@lanl.gov, rweinmann@lanl.gov

² Nuclear Engineering Department, University of Florida, Gainesville, FL 32611, USA
E-mail: enqvist@mse.ufl.edu

³ Safeguards and Security Technology, Nuclear Security & Isotope Division, Oak Ridge National Laboratory, One Bethel Valley road, Oak Ridge, TN 37831, USA
E-mail: crofts@ornl.gov
LA-UR-17-22582

Abstract:

Lightly encapsulated ^{252}Cf sources are commonly used to characterize and calibrate neutron detectors for safeguards applications without much attention being paid to what it means for the encapsulation to be neutronically "light". In this work we quantify the impact of encapsulation on both the neutron spectrum and neutron intensity. We find that a 1.3 mm shell of copper reduces the mean energy by about 1 %. Thus encapsulation can be used to deliberately adjust the mean energy to match, for example, that of the spontaneously fissile Pu nuclides. The spectrum cannot be matched perfectly however and so the influence of encapsulation on a particular system calibration is case specific. We demonstrate using encapsulation to match the Pu neutron detection efficiency for a common safeguards detector, the Active Well Coincidence Counter.

Keywords: NDA; Monte Carlo; Prompt Fission Neutron Spectrum, ^{252}Cf , encapsulation

1. Introduction

Monte Carlo modeling is a well established way to make performance estimates of neutron assay systems for safeguards [1]. The models may be benchmarked against experimental results obtained using sealed sources containing ^{252}Cf , which is a convenient source of spontaneous fission neutrons, as a surrogate for the materials of interest. Often a correction is needed to allow for the difference between the energy spectrum of the ^{252}Cf neutrons and the neutron emission spectrum of interest [2]. For a bare ^{252}Cf source the prompt fission neutron spectrum from ^{252}Cf may be approximated reasonably well by simple analytical shapes. For instance in ISO 8529 [3] a Maxwellian distribution with a temperature parameter of 1.42 MeV corresponding to a mean energy of 2.13 MeV is recommended. Fröhner [4] makes the case for the next simplest macroscopic representation, namely the Watt spectrum, with a temperature parameter equal to 1.175 MeV and the fragment kinetic energy per nucleon parameter of 0.359 MeV corresponding to a mean energy of approximately 2.122 MeV. These approximations are valid for lightly

encapsulated ^{252}Cf sources, but the meaning of light encapsulation is not quantified in the literature. Presumably the Amersham X1 capsule [5] would qualify. This is a cylindrical assembly about 10 mm long and 7.8 mm in diameter with a combined wall thickness of roughly 1.6 mm of stainless steel. But it is well established that even such a modest capsule perturbs the angular distribution from what would otherwise be a near perfect isotropic pattern. The neutrons emitted isotropically by a small amount of ^{252}Cf source material exit the capsule in an anisotropic distribution with near cylindrical symmetry about the axis of the capsule [5,6]. When calibrating a fluence measuring device correction factors for the anisotropic emission of the source must be made [5-8]. Less well known is the impact on the neutron spectrum caused by neutron interactions in the source encapsulation. Whether the difference between a 1 mm and a 3 mm stainless steel container, or some other jacketing material, matters or not clearly depends on the detailed response function of the system. However, the lack of general guidance on what constitutes a lightly encapsulated source and the general neglect of the effect of encapsulation on the neutron spectrum in the scientific literature means it is difficult to make an informed judgment. In this work we take a step to resolving this dilemma by analyzing the effect of encapsulation on a specific system. In Section 2 we present a simple analysis justifying why encapsulation needs to be considered in neutron metrology and establishing that for common source types spectral indices might be expected to exhibit a linear behavior with wall thickness. In Section 3 we draw on published results taken from a report [9] in which the authors were deliberately trying to moderate the spectrum of ^{252}Cf and $^{241}\text{Am}/\text{Be}(\alpha, n)$ sources as an alternative to using accelerator facilities to obtain a variety of spectra for calibration of neutron dosimetry instruments. In particular we show how the mean energy from ^{252}Cf surrounded by spherical shells scales roughly linearly with shell thickness. In real situations we are concerned with the full energy distribution, as modified by all reaction channels, and also with potential losses and gains to the number of neutrons emerging per initial source neutron. This was studied in Section 4 through a series of Monte Carlo simulations using the Los Alamos MCNP6 code [9, 10]. The effects of spheres of

common materials were simulated, along with some common commercial encapsulations. Finally the spectrum modification was coupled to the Active Well Multiplicity Counter (AWCC) [12 detection efficiency, and the source encapsulation was modified to match the detection efficiency of ^{240}Pu . Manufactured cylindrical encapsulation was measured for verification.

2. A simple analysis

We might intuitively expect that simple spectral indices of the emergent neutron spectrum will vary linearly with the thickness of the encapsulation when the thickness is small. Consider as an example how the mean energy for a point emitter located at the centre of a thin spherical shell of encapsulating material will shift as a function of shell thickness under the approximation that the only reaction of significance taking place is elastic scattering. Because of the assumption that the source is lightly encapsulated the probability, p_s , that a neutron will scatter on its way out is given, to first order, by

$$p_s = \Sigma_s t \ll 1$$

where Σ_s is the macroscopic scattering cross section of the shell material and t is its thickness.

Thus, a fraction $(1 - p_s)$ of neutrons emerge without scattering and without suffering any energy loss. The neutrons that do scatter will lose on average an energy of half the amount of the maximum energy that can be transferred to the target nucleus as recoil kinetic energy under the additional assumption that the scattering is isotropic in the center of mass reference frame. Thus, we can write the mean fractional neutron energy loss, f , as

$$f = \frac{2A}{(1+A)^2}$$

where A is the ratio of the mass of the target nucleus to that of the rest mass of the neutron. For an element we may take, to a good approximation, A to be numerically equal to the molar mass in $\text{g}\cdot\text{mol}^{-1}$.

The mean energy of the scattered neutrons, \bar{E}_s , is consequently lower than the mean energy, \bar{E} , of the emitting source and can be expressed as

$$\bar{E}_s = \bar{E}(1-f) = \bar{E} \left(1 - \frac{2A}{(1+A)^2} \right)$$

The mean energy of the emerging spectrum of neutrons, \bar{E}_{ext} , is formed from the contributions of both the unscattered and scattered neutrons and becomes

$$\bar{E}_{ext} = (1-p_s)\bar{E} + p_s\bar{E}_s = (1-p_s)\bar{E} + p_s\bar{E} \left(1 - \frac{2A}{(1+A)^2} \right)$$

which upon rearrangement and substitution yields

$$\bar{E}_{ext} = \bar{E} \left(1 - \frac{2A}{(1+A)^2} \Sigma_s t \right)$$

This formula predicts that for an idealized scattering capsule the mean emergent energy will fall linearly with wall thickness. Real capsules can drop energies more effectively

through inelastic processes and other channels such as $(n,2n)$ interactions. The latter is also an example of a neutron gain process, in contrast (n,α) interactions are an example of a neutron loss process. Although we did not consider these kinds of interaction in the simple view presented, for a thin wall, the basic idea remains sound. Thus, we anticipate the ratio between the emergent mean energy and that of the ideal unencapsulated source to trend roughly as follows

$$R = \frac{\bar{E}_{ext}}{\bar{E}} = 1 - bt$$

where b is a coefficient specific to the composition and density of the wall material.

3. Illustration using literature data

Hsu and Chen [9] performed a series of calculations in which ^{252}Cf was placed at the center of spheres of various radii and of various materials to see if they could create reference spectra that would be useful for calibrating health physics instruments. Spheres of radius 25.4, 50.8, 76.2, 101.6, 153.2 and 203.2 mm were selected. Twelve materials were studied Be, graphite, Al, Fe, Cu, Pb, LiD, H_2O , D_2O , polyethylene $(\text{CH}_2)_n$, glass and concrete. Neutron spectra at 500 mm from the center were computed. The results are presented graphically and are difficult to interpret. Gains and losses are not quantified. The mean energy as a function of wall thickness is given numerically only in the case of copper. With zero wall thickness the mean energy is given as 2.54 MeV. This is far higher than the generally accepted value of about 2.12 to 2.13 MeV [2,3]. However, by forming the ratio of the emergent spectrum to the initiating spectrum we expect that this apparent bias will be largely suppressed. The data was fit to the form

$$R = e^{-bt}$$

which reduces to the linear form ($R \approx 1 - bt$) expected for thin shell walls when $bt \ll 1$.

In the present case the exponential fit produces an excellent fit across the whole range of spheres modeled with $b = 0.0079 \text{ mm}^{-1}$ and an R^2 value of 0.99992, as evident in Figure 1. The uncertainty in the b value is unknown because uncertainties were not reported in the original work. It is also apparent from Figure 1 that a copper sphere with a radius greater than about 10 or 20 mm cannot be considered thin in the context of our earlier simple theoretical development. A radius (wall thickness) of a few mm falls in the linear range and we see that to get a 1% shift in mean energy requires a wall thickness of about $0.01/0.0079 = 1.27$ mm of Cu; this equates to a shift of about 21 keV in the mean energy. For the HLNCC-II [13], a common thermal well counter with a single ring of ^3He filled proportional counters, the fractional change in detection efficiency in the vicinity of 2 MeV is about 17% per MeV [14]. Thus a 21 keV reduction in mean energy translates into a projected relative increase in efficiency of about 0.36% (from about 0.1750 counts per neutron to about 0.1756 counts per neutron. This is a change which is readily measurable.

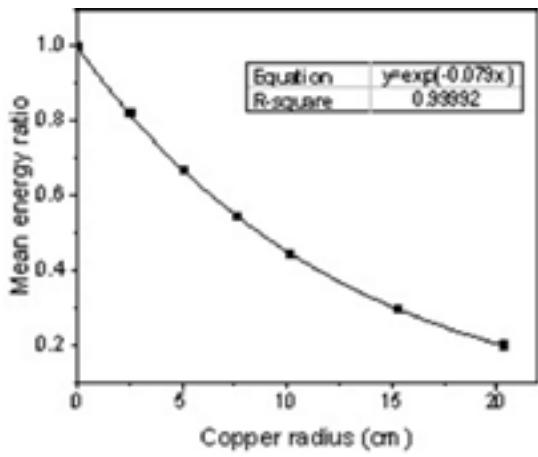


Figure 1: Plot of mean energy ratio, R , as a function of moderator radius, t , taken from [9] for the case of ^{252}Cf at the center of Cu spheres along with the fitted result.

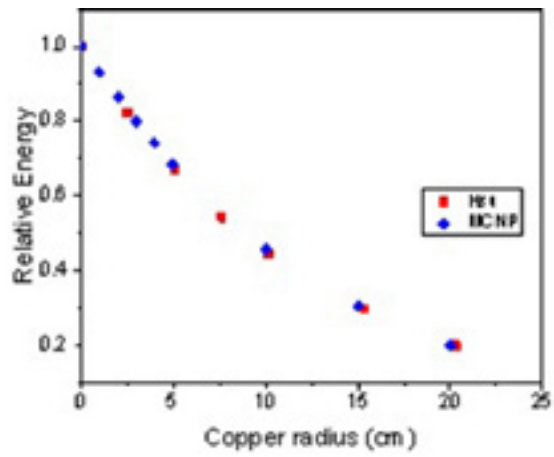


Figure 2: Comparison of our MCNP calculations and the results of Hsu et al [9] interpreted as a relative energy to remove the obvious mean energy discrepancy in that work.

4. Detailed modeling

Although instructive the results of Hsu and Chen do not cover the range of interest relevant to our present discussion – which is the use of lightly encapsulated sources typical of those obtained from a variety of vendors and used routinely in safeguards laboratories. For this reason we performed a series of focused Monte Carlo simulations. These calculations give not only the mean energy shift but the shape of the spectrum and also allow losses and gains to be tallied.

The model used the MCNP6.1.1b default energy spectrum of spontaneous fission of ^{252}Cf with a mean energy of 2.13 MeV, corresponding to Watt spectrum parameters of $a=1.180$ MeV and $b=1.03419$ MeV⁻¹. Coincidence counting was not simulated, so default physics options including non-analog transport were used. The neutrons were started at a point source at the origin. The energy was tallied over a sphere centered at the origin with a radius of 300 mm. Figure 2 shows the average energy of

neutrons crossing this sphere as a function of thickness of copper. The results of Hsu are also included in the figure, and both show the same general trend. The mean energy of prompt fission neutrons from ^{240}Pu spontaneous fission, again using the default MCNP6.1.1b spontaneous fission energy spectrum is 1.93 MeV. Using the exponential relationship shown in Figure 2, we would require a sphere of 13.9mm copper thickness to produce an average energy equal to that of a notional bare ^{240}Pu source.

Table 1 shows the gains, losses, net neutrons, and average energy, for spheres of the materials calculated in MCNP for thicknesses between 1 and 20 cm. The gains, losses, and net values are per source neutron. Lead has the least effect on the average energy while polyethylene has the most. Beryllium's (n,2n) reaction causes a 6.5% increase in emitted neutrons at a thickness of 15 cm. Stainless steel has a negligible net intensity effect but a potentially significant energy effect at the thicknesses of common encapsulations.

Aluminum				
Spherical Radius (cm)	Gains	Losses	Net	Average energy (MeV)
1	6.28*10 ⁻⁷	3.82*10 ⁻⁴	1.00*10 ⁰	2.07*10 ⁰
2	1.22*10 ⁻⁶	7.50*10 ⁻⁴	9.99*10 ⁻¹	2.02*10 ⁰
3	1.73*10 ⁻⁶	1.11*10 ⁻³	9.99*10 ⁻¹	1.96*10 ⁰
4	2.22*10 ⁻⁶	1.45*10 ⁻³	9.99*10 ⁻¹	1.91*10 ⁰
5	2.64*10 ⁻⁶	1.79*10 ⁻³	9.98*10 ⁻¹	1.85*10 ⁰
10	4.25*10 ⁻⁶	3.33*10 ⁻³	9.97*10 ⁻¹	1.58*10 ⁰
15	5.71*10 ⁻⁶	4.70*10 ⁻³	9.95*10 ⁻¹	1.32*10 ⁰
20	6.66*10 ⁻⁶	6.00*10 ⁻³	9.94*10 ⁻¹	1.08*10 ⁰

Beryllium				
Spherical Radius (cm)	Gains	Losses	Net	Average energy (MeV)
1	3.07*10 ⁻²	2.00*10 ⁻²	1.01*10 ⁰	2.00*10 ⁰
2	5.87*10 ⁻²	3.83*10 ⁻²	1.02*10 ⁰	1.87*10 ⁰
3	8.41*10 ⁻²	5.50*10 ⁻²	1.03*10 ⁰	1.74*10 ⁰
4	1.07*10 ⁻¹	7.05*10 ⁻²	1.04*10 ⁰	1.60*10 ⁰
5	1.28*10 ⁻¹	8.50*10 ⁻²	1.04*10 ⁰	1.47*10 ⁰
10	2.02*10 ⁻¹	1.37*10 ⁻¹	1.06*10 ⁰	8.78*10 ⁻¹
15	2.43*10 ⁻¹	1.78*10 ⁻¹	1.07*10 ⁰	4.79*10 ⁻¹
20	2.65*10 ⁻¹	2.28*10 ⁻¹	1.04*10 ⁰	2.48*10 ⁻¹
Concrete				
Spherical Radius (cm)	Gains	Losses	Net	Average energy (MeV)
1	8.84*10 ⁻⁷	9.42*10 ⁻⁴	9.99*10 ⁻¹	2.05*10 ⁰
2	1.47*10 ⁻⁶	1.85*10 ⁻³	9.98*10 ⁻¹	1.97*10 ⁰
3	2.06*10 ⁻⁶	2.74*10 ⁻³	9.97*10 ⁻¹	1.88*10 ⁰
4	2.72*10 ⁻⁶	3.61*10 ⁻³	9.96*10 ⁻¹	1.80*10 ⁰
5	3.21*10 ⁻⁶	4.48*10 ⁻³	9.96*10 ⁻¹	1.71*10 ⁰
10	1.04*10 ⁻⁵	1.27*10 ⁻²	9.87*10 ⁻¹	1.29*10 ⁰
15	6.38*10 ⁻⁴	4.96*10 ⁻²	9.50*10 ⁻¹	9.21*10 ⁻¹
20	5.81*10 ⁻³	1.38*10 ⁻¹	8.62*10 ⁻¹	6.41*10 ⁻¹
Copper				
Spherical Radius (cm)	Gains	Losses	Net	Average energy (MeV)
1	5.19*10 ⁻⁵	2.22*10 ⁻³	9.98*10 ⁻¹	1.98*10 ⁰
2	9.91*10 ⁻⁵	4.61*10 ⁻³	9.95*10 ⁻¹	1.84*10 ⁰
3	1.42*10 ⁻⁴	7.22*10 ⁻³	9.93*10 ⁻¹	1.70*10 ⁰
4	1.82*10 ⁻⁴	1.01*10 ⁻²	9.90*10 ⁻¹	1.58*10 ⁰
5	2.14*10 ⁻⁴	1.32*10 ⁻²	9.87*10 ⁻¹	1.46*10 ⁰
10	3.25*10 ⁻⁴	3.48*10 ⁻²	9.65*10 ⁻¹	9.75*10 ⁻¹
15	3.82*10 ⁻⁴	7.05*10 ⁻²	9.30*10 ⁻¹	6.47*10 ⁻¹
20	4.07*10 ⁻⁴	1.25*10 ⁻¹	8.75*10 ⁻¹	4.26*10 ⁻¹
Heavy water				
Spherical Radius (cm)	Gains	Losses	Net	Average energy (MeV)
1	8.53*10 ⁻⁴	7.43*10 ⁻⁴	1.00*10 ⁰	1.98*10 ⁰
2	1.64*10 ⁻³	1.44*10 ⁻³	1.00*10 ⁰	1.83*10 ⁰
3	2.38*10 ⁻³	2.16*10 ⁻³	1.00*10 ⁰	1.68*10 ⁰
4	3.06*10 ⁻³	2.69*10 ⁻³	1.00*10 ⁰	1.54*10 ⁰
5	3.69*10 ⁻³	3.24*10 ⁻³	1.00*10 ⁰	1.40*10 ⁰
10	6.20*10 ⁻³	5.46*10 ⁻³	1.00*10 ⁰	8.54*10 ⁻¹
15	7.85*10 ⁻³	7.03*10 ⁻³	1.00*10 ⁰	5.02*10 ⁻¹
20	8.92*10 ⁻³	8.39*10 ⁻³	1.00*10 ⁰	2.91*10 ⁻¹
Iron				
Spherical Radius (cm)	Gains	Losses	Net	Average energy (MeV)
1	3.25*10 ⁻⁵	8.69*10 ⁻⁴	9.99*10 ⁻¹	2.02*10 ⁰
2	6.05*10 ⁻⁵	1.70*10 ⁻³	9.98*10 ⁻¹	1.91*10 ⁰
3	8.59*10 ⁻⁵	2.56*10 ⁻³	9.97*10 ⁻¹	1.80*10 ⁰
4	1.10*10 ⁻⁴	3.41*10 ⁻³	9.97*10 ⁻¹	1.70*10 ⁰
5	1.31*10 ⁻⁴	4.28*10 ⁻³	9.96*10 ⁻¹	1.60*10 ⁰
10	2.03*10 ⁻⁴	8.90*10 ⁻³	9.91*10 ⁻¹	1.18*10 ⁰
15	2.43*10 ⁻⁴	1.40*10 ⁻²	9.86*10 ⁻¹	8.79*10 ⁻¹
20	2.61*10 ⁻⁴	2.05*10 ⁻²	9.80*10 ⁻¹	6.77*10 ⁻¹

Glass				
Spherical Radius (cm)	Gains	Losses	Net	Average energy (MeV)
1	7.80×10^{-7}	1.23×10^{-3}	9.99×10^{-1}	2.09×10^0
2	1.34×10^{-6}	2.43×10^{-3}	9.98×10^{-1}	2.04×10^0
3	2.14×10^{-6}	3.62×10^{-3}	9.96×10^{-1}	1.99×10^0
4	2.84×10^{-6}	4.78×10^{-3}	9.95×10^{-1}	1.95×10^0
5	3.53×10^{-6}	5.92×10^{-3}	9.94×10^{-1}	1.90×10^0
10	6.15×10^{-6}	1.12×10^{-2}	9.89×10^{-1}	1.65×10^0
15	8.30×10^{-6}	1.59×10^{-2}	9.84×10^{-1}	1.39×10^0
20	9.46×10^{-6}	2.00×10^{-2}	9.80×10^{-1}	1.14×10^0
Graphite				
Spherical Radius (cm)	Gains	Losses	Net	Average energy (MeV)
1	0.00×10^0	1.37×10^{-4}	1.00×10^0	2.08×10^0
2	0.00×10^0	2.66×10^{-4}	1.00×10^0	2.02×10^0
3	0.00×10^0	3.87×10^{-4}	1.00×10^0	1.96×10^0
4	0.00×10^0	5.01×10^{-4}	9.99×10^{-1}	1.90×10^0
5	0.00×10^0	6.09×10^{-4}	9.99×10^{-1}	1.84×10^0
10	0.00×10^0	1.06×10^{-3}	9.99×10^{-1}	1.50×10^0
15	0.00×10^0	1.42×10^{-3}	9.99×10^{-1}	1.17×10^0
20	0.00×10^0	1.92×10^{-3}	9.98×10^{-1}	8.67×10^{-1}
Water				
Spherical Radius (cm)	Gains	Losses	Net	Average energy (MeV)
1	0.00×10^0	3.28×10^{-4}	1.00×10^0	1.94×10^0
2	0.00×10^0	8.30×10^{-4}	9.99×10^{-1}	1.75×10^0
3	0.00×10^0	3.11×10^{-3}	9.97×10^{-1}	1.57×10^0
4	0.00×10^0	1.14×10^{-2}	9.89×10^{-1}	1.41×10^0
5	0.00×10^0	3.06×10^{-2}	9.69×10^{-1}	1.25×10^0
10	6.62×10^{-8}	3.06×10^{-1}	6.94×10^{-1}	6.93×10^{-1}
15	1.99×10^{-8}	6.25×10^{-1}	3.75×10^{-1}	3.79×10^{-1}
20	1.99×10^{-8}	8.17×10^{-1}	1.83×10^{-1}	2.08×10^{-1}
Lead				
Spherical Radius (cm)	Gains	Losses	Net	Average energy (MeV)
1	5.24×10^{-4}	2.62×10^{-4}	1.00×10^0	2.07×10^0
2	1.01×10^{-3}	6.06×10^{-4}	1.00×10^0	2.00×10^0
3	1.46×10^{-3}	9.46×10^{-4}	1.00×10^0	1.94×10^0
4	1.88×10^{-3}	1.25×10^{-3}	1.00×10^0	1.88×10^0
5	2.27×10^{-3}	1.13×10^{-3}	1.00×10^0	1.83×10^0
10	3.80×10^{-3}	2.98×10^{-2}	1.00×10^0	1.56×10^0
15	4.81×10^{-3}	4.51×10^{-3}	1.00×10^0	1.33×10^0
20	5.45×10^{-3}	6.31×10^{-2}	9.99×10^{-1}	1.14×10^0
Lithium deuteride				
Spherical Radius (cm)	Gains	Losses	Net	Average energy (MeV)
1	7.71×10^{-4}	1.89×10^{-3}	9.98×10^{-1}	1.95×10^0
2	1.45×10^{-3}	4.65×10^{-3}	9.96×10^{-1}	1.77×10^0
3	2.07×10^{-3}	9.46×10^{-3}	9.93×10^{-1}	1.61×10^0
4	2.62×10^{-3}	1.35×10^{-2}	9.88×10^{-1}	1.44×10^0
5	3.11×10^{-3}	2.03×10^{-2}	9.81×10^{-1}	1.29×10^0
10	4.84×10^{-3}	1.00×10^{-1}	9.02×10^{-1}	7.06×10^{-1}
15	5.82×10^{-3}	2.71×10^{-1}	7.32×10^{-1}	3.62×10^{-1}
20	6.35×10^{-3}	4.78×10^{-1}	5.25×10^{-1}	1.79×10^{-1}

Polyethylene				
Spherical Radius (cm)	Gains	Losses	Net	Average energy (MeV)
1	0.00*10 ⁰	8.30*10 ⁻⁵	1.00*10 ⁰	1.89*10 ⁰
2	0.00*10 ⁰	9.10*10 ⁻⁴	9.99*10 ⁻¹	1.66*10 ⁰
3	0.00*10 ⁰	7.62*10 ⁻³	9.92*10 ⁻¹	1.44*10 ⁰
4	0.00*10 ⁰	2.98*10 ⁻²	9.70*10 ⁻¹	1.25*10 ⁰
5	0.00*10 ⁰	7.39*10 ⁻²	9.26*10 ⁻¹	1.08*10 ⁰
10	0.00*10 ⁰	4.81*10 ⁻¹	5.19*10 ⁻¹	5.02*10 ⁻¹
15	0.00*10 ⁰	7.83*10 ⁻¹	2.17*10 ⁻¹	2.34*10 ⁻¹
20	0.00*10 ⁰	9.14*10 ⁻¹	8.59*10 ⁻²	1.12*10 ⁻¹
Stainless Steel				
Spherical Radius (cm)	Gains	Losses	Net	Average energy (MeV)
1	3.28*10 ⁻⁵	1.47*10 ⁻³	9.99*10 ⁻¹	2.01*10 ⁰
2	6.29*10 ⁻⁵	2.91*10 ⁻³	9.97*10 ⁻¹	1.89*10 ⁰
3	8.88*10 ⁻⁵	4.34*10 ⁻³	9.96*10 ⁻¹	1.78*10 ⁰
4	1.12*10 ⁻⁴	5.77*10 ⁻³	9.94*10 ⁻¹	1.67*10 ⁰
5	1.32*10 ⁻⁴	7.18*10 ⁻³	9.93*10 ⁻¹	1.57*10 ⁰
10	2.06*10 ⁻⁴	1.45*10 ⁻²	9.86*10 ⁻¹	1.13*10 ⁰
15	2.43*10 ⁻⁴	2.39*10 ⁻²	9.76*10 ⁻¹	8.23*10 ⁻¹
20	2.64*10 ⁻⁴	3.87*10 ⁻²	9.61*10 ⁻¹	6.10*10 ⁻¹

Table 1: Effects of spherical encapsulation of various materials on a Cf-252 source.

4.1 Commercial encapsulation

While the previous information is interesting academically, most source encapsulation encountered is standard manufactured capsules from source vendors. Variations in the capsules are introduced through spacers in the source cavity void, inner and outer capsules of different materials, and the inclusion of threaded studs or other modifications. 304L Stainless steel is the most common capsule material in our experience, but Zircalloy-2 is also used.

Physical information about the capsules as simulated is described in Table 2. The A3026 capsule is provided by Eckert & Ziegler [15]. The FTC capsules are provided by

Frontier Technology Corporation [16], where s denotes a shorter version of the capsule. The FTC 10 capsules are single encapsulation. The FTC 100 capsule is the second encapsulation that surrounds a FTC 10 capsule and both were included in the simulations. FTC 10 and FTC 100 are the equivalent of Savannah River National Laboratory's SR-Cf-1X and SR-CF-100 capsules respectively. X1 capsules are provided by Amersham, now known as QSA [17]. Table 2 shows the physical characteristics and Table 3 shows the gains, losses, net, and average energy of the spectrum. Simulations demonstrated a negligible difference between 304 and 304L SS, which is to be expected as only the concentration of carbon atoms (less than 1% overall) change.

Capsule	Material	Mass (g)	Outer diameter (cm)	Outer length (cm)
A3026	304 SS	18.4	0.942	3.6
FTC 10s	304L SS	1.7	0.551	1.19
FTC 10	304L SS	2.9	0.551	2.46
FTC 100	304L SS	15.9	0.942	3.76
Amersham X1	SS	3.1	0.782	0.98

Table 2: Common encapsulation's physical characteristics.

Capsule	Gains	Losses	Net	Average energy (MeV)
A3026	1.816*10 ⁻⁵	7.563*10 ⁻⁴	9.993*10 ⁻¹	2.067
FTC 10s	5.643*10 ⁻⁶	2.221*10 ⁻⁴	9.998*10 ⁻¹	2.112
FTC 10	5.111*10 ⁻⁶	2.072*10 ⁻⁴	9.998*10 ⁻¹	2.113
FTC 100	1.411*10 ⁻⁵	5.760*10 ⁻⁴	9.994*10 ⁻¹	2.083
Amersham X1	1.012*10 ⁻⁵	4.476*10 ⁻⁴	9.996*10 ⁻¹	2.100

Table 3: Common encapsulation's effects on the emergent neutrons.

Figure 3 shows the emission spectra of bare ^{240}Pu and bare ^{252}Cf together with the calculated spectrum from a point ^{252}Cf source inside a 13.9 mm radius sphere of copper. Although the mean energy can be easily matched, the spectra show that the shape of the tailored spectrum is non-the-less significantly different from that of ^{240}Pu . Whether this is important depends on the nature of the measurement configuration and the objectives of the experiment. For detectors with non-linear response functions matching the average energy is insufficient to match the measurement efficiency. For example a detector with a peak detection efficiency at 1 MeV will have a different efficiency for neutrons at only 1 MeV compared to neutrons half at 0.5 MeV and half at 1.5 MeV.

4.2 Effects in the AWCC

A complete analysis of the effects of encapsulation is detector specific. The Active Well Coincidence Counter (AWCC) was simulated to find the encapsulation of ^{252}Cf necessary to match the ^{240}Pu efficiency and measurements were made to verify the simulations. A plot of the simulation with one polyethylene shell is shown in Figure 4. A series of measurements were taken with cylindrical encapsulation of varying wall thicknesses of stainless steel, copper, and polyethylene. The encapsulations are shown in Figure 5. The ^{252}Cf source was Isotope Product Laboratories' A7-869 in the A3026 capsule. First, the exit spectra of the capsules were simulated. Then the measured and simulated ring ratios of the total neutron counts in the AWCC were compared. The AWCC non-linear detection efficiency as a function of neutron energy was simulated. Finally the AWCC measured and simulated efficiencies are compared, and an estimation of the encapsulation to match ^{240}Pu efficiency is given.

The AWCC can operate in thermal mode without thermal neutron absorbers or in fast mode with cadmium liners and a nickel reflection ring. In fast mode the sample cavity cadmium liner reduces the count rate in high mass samples and the cadmium liners of the interrogation source ensure a high energy interrogation flux for better penetration of large samples. In this study the fast mode was used. The cadmium liners of 1.6 mm thickness absorb neutrons below about 0.7 eV.

The exit ^{252}Cf spectra from the capsules are shown in Figure 6. The results show that increasing encapsulation amplifies the change in spectrum. The strong thermalization efficiency of polyethylene is demonstrated by the increasing flux at lower energies, indicating a relatively bimodal distribution compared to the other materials. The absorption resonances in copper at 0.002 MeV and other energies can be seen.

The AWCC has two rings of ^3He detectors at different depths of polyethylene as shown in Figure 7, so as neutrons in a specific energy range are moderated their

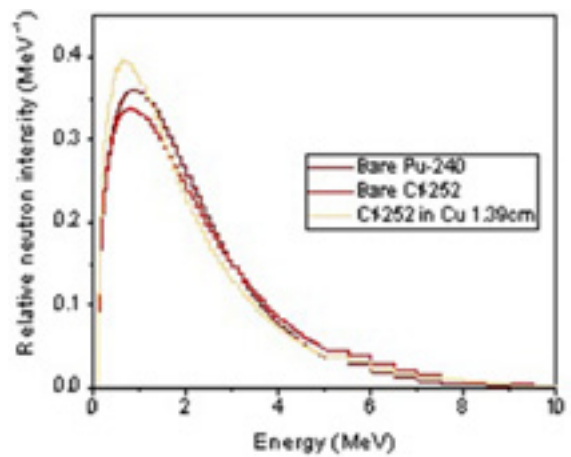


Figure 3: Normalized Spectra from bare ^{240}Pu , bare ^{252}Cf and ^{252}Cf within a 13.9 mm copper sphere

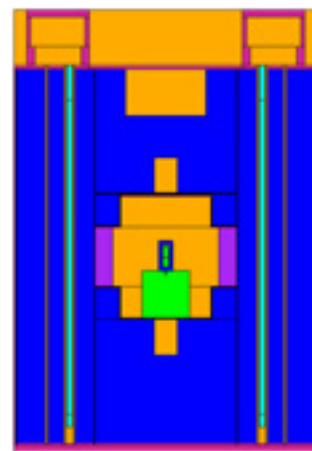


Figure 4: MCNP6 simulation of the AWCC in fast mode with one polyethylene shell.



Figure 5: Encapsulations with wall thicknesses of 0.5 cm.

detection efficiency by one ring goes up while the other goes down, dampening the change in overall detector efficiency. This effect is more pronounced in neutron detectors with more rings, while single ringed neutron detectors such as the HLNCC-II [13] are more susceptible to changes in the source energy spectrum.

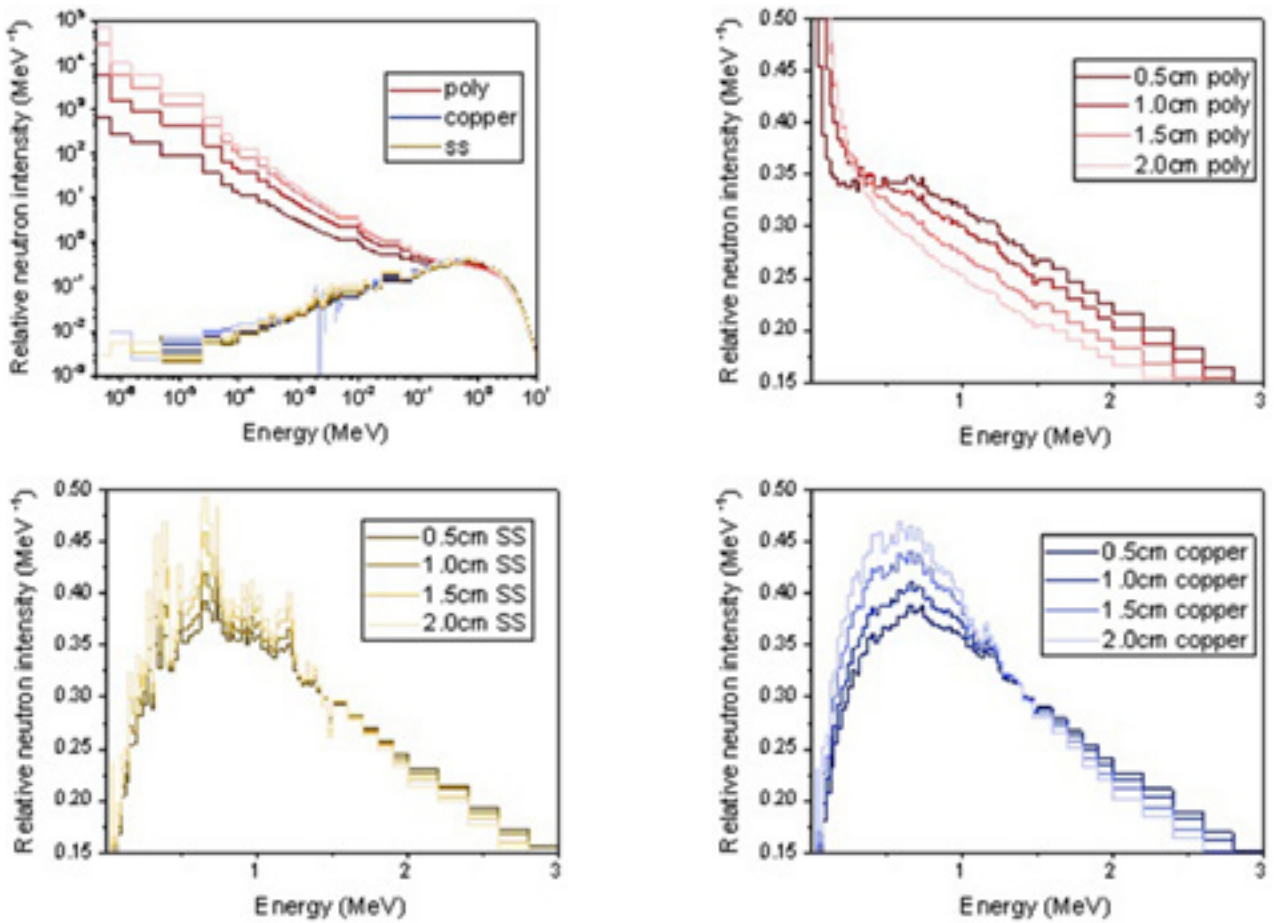


Figure 6: Exit spectra of encapsulation. Note the log-log scale in the first figure. Individual materials are shown in a range of 0-3 MeV on a linear scale.

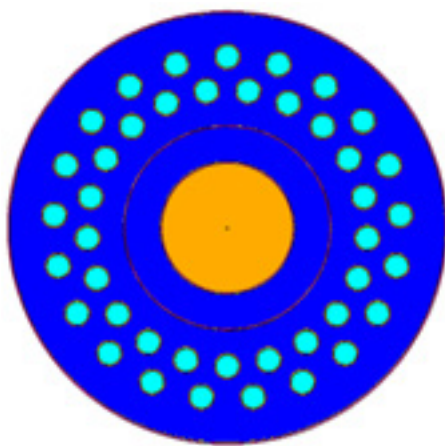


Figure 7: Top down view of the AWCC design.

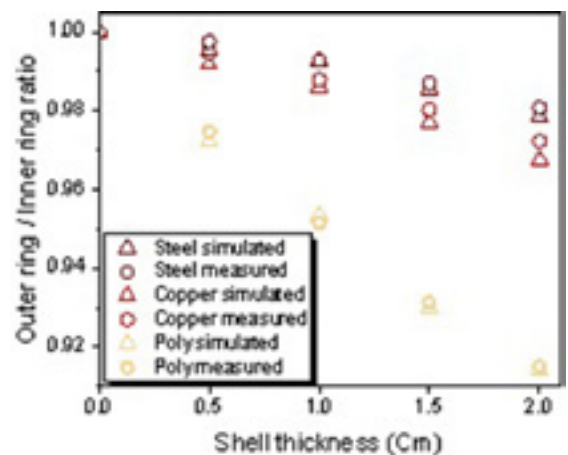


Figure 8: Measured and simulated AWCC ring ratios relative to the bare A7-869 source for various encapsulations.

The measurements and simulations of the ring ratio were compared to verify the accuracy of the simulations. Generally, the ratio of the neutron counts of the two AWCC rings indicates the detected neutron energy. Higher energy neutrons are more likely to reach the outer ring before being absorbed in the inner ring, and so the ratio of counts detected depends on the energy spectrum emitted by the

source. The ratio is independent of the source strength, which is a major source of uncertainty in comparing measurements to MCNP simulations. The values were normalized to the ratio of only the standard A3026 source encapsulation to remove bias in the simulation of the detector. The results are shown in Figure 8. The relative statistical uncertainty was too small to clearly plot and was less than

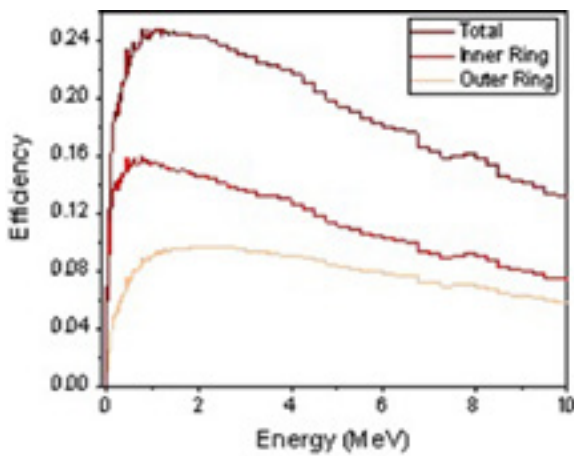


Figure 9: AWCC response function.

0.02% for measurements and 0.09% for simulations. The measurements and simulations agree within 2 standard deviations for all cases except the 2 cm shell thickness of copper. The strong agreement demonstrates that the simulation accurately simulates the measurement.

The AWCC response function, the efficiency as a function of neutron energy emitted by the source, was simulated and is shown in Figure 9. The AWCC response function demonstrates how a neutron spectrum's mean energy does not directly correspond to the efficiency. A spectrum of neutrons half at 0.5 MeV and half at 2.5 MeV will have a lower efficiency than neutrons at their average of 1.5 MeV. The simulation shows that the peak efficiency is around 1.2 MeV. The inner ring has a higher efficiency due to moderation and geometric considerations and its peak efficiency occurs at a neutron energy of about 0.6 MeV while the outer ring peak efficiency occurs at about 2.1 MeV.

Finally, measurements and simulations of the AWCC detection efficiency can be compared to demonstrate the encapsulation's effect on the detector response. Agreement of measurements and simulations indicates the accuracy of the simulations. The simulations can then be used to model measurements that were unavailable to perform physically, like a bare ^{252}Cf source with no encapsulation. It is important to compare encapsulation's effects on detection efficiency, not on average energy. The result of the comparison is shown in Figure 10 and is normalized to the efficiency of the A7-869 source in the A3026 capsule. The relative uncertainties were 0.07% for the simulations and 0.02% for the measurements, which are too small to appear in the figure.

The ^{252}Cf encapsulation required to match the detection efficiency of ^{240}Pu was calculated. The simulations of a bare ^{240}Pu source and a bare ^{252}Cf source give relative efficiencies of 0.992 and 0.980, compared to ^{252}Cf in an A3026 capsule. The difference between the absolute detection

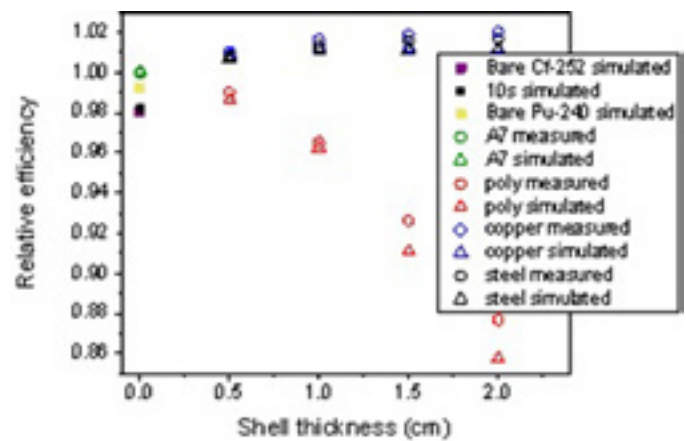


Figure 10: Simulated and measured efficiencies normalized to the A7-869 source in A3026 encapsulation.

efficiency of ^{252}Cf and ^{240}Pu is 0.23%, but the values of absolute detection efficiency are not reported because of uncertainties in the source strength and bias in the simulations. Adding the A3026 capsule increases the relative efficiency to 1, and an additional 0.5cm of polyethylene around the A3026 capsule reduces the relative efficiency to 0.986, which differs from the ^{240}Pu relative efficiency by -0.006 and differs by a ^{240}Pu absolute efficiency of -0.13%. A polyethylene shell thickness of 0.35cm gives a relative efficiency of 0.992 compared to A3026 encapsulation. The absolute efficiency differs from that of ^{240}Pu by 0.004% which is within one sigma uncertainty. In other words, 0.35cm of polyethylene around a ^{252}Cf source in an A3026 capsule will match the AWCC detection efficiency of ^{240}Pu .

5. Conclusion

A few mm of metallic encapsulation influences the energy spectrum emerging from ^{252}Cf to a degree that is measurable in safeguards systems. This also means that the average energy of a point ^{252}Cf spontaneous fission neutron source can be tailored to match any lower value. This is a useful feature to exploit when using ^{252}Cf to measure the neutron detector efficiency as a surrogate for Pu sources in cases where the detector response is a simple function of energy. The modified spectrum however shows significant differences from a Pu spectrum with the same average energy and thus is unlikely to be adequate for detectors with strongly non-linear energy efficiency profiles. In non-linear response detectors such as the Active Well Coincidence Counter, Monte Carlo simulations can be used to calculate the encapsulation needed. In the AWCC a cylindrical encapsulation of polyethylene around an A7-series source with a wall thickness of 0.35cm will match the efficiency of a bare ^{240}Pu pure fission source. Conversely, this information shows the effects of unwanted encapsulation and guides the user towards a decision about an encapsulation being 'neutronically light'.

Acknowledgements

This work was sponsored in part by the U.S. Department of Energy (DOE), National Nuclear Security Administration (NNSA), Office of Nonproliferation and Verification Research and Development (NA-22). This work was funded in part by the Consortium for Verification Technology under Department of Energy National Nuclear Security Administration award number DE-NA0002534.

References

- [1] Menlove, H. O, Swinhoe, M. T., Rinard, P. M., Calibration of Pu and Cm Detectors using ^{252}Cf . Los Alamos Report LA-13961-MS. (2002)
- [2] Croft, S., Favalli, A., Swinhoe, M.T. and Rael, C.D., State of the art Monte Carlo modeling of active collar measurements and comparison with experiment, Proc. 52nd Annual INMM Meeting, Palm Desert, CA, USA, July 2011
- [3] International Organization for Standardization, Reference neutron radiations -- Part 1: Characteristics and Methods of Production, ISO 8529-1:2001-02-01(E), see also ISO 8529-1:2001/Cor 1:2008(F) which provide a typographical correction to Table A.4 the $^{241}\text{Am}\text{-Be}(\alpha,n)$ spectrum. (2001)
- [4] Fröhner, F.H., Evaluation of ^{252}Cf prompt fission neutron data from 0 to 20 MeV by Watt spectrum fit, Nuclear Science and Engineering 106 (1990) 345-352.
- [5] Bardell, A.G., Burke, M., Hunt, J.B., Tagziria H., and Thomas, D.J., Anisotropy of emission from radionuclide neutron sources, National Physical Laboratory report CIRM 24, ISSN 1369-6793. Dec. 1998.
- [6] Tsujimura, N., Yoshida, T., and Momose, T., Calculations of anisotropy factors for radionuclide neutron sources due to scattering from encapsulation and support structures, Radiat. Prot. Dosim. 126(1-4) (2007) 168-173.
- [7] Hawkes N.P., Freedman R., Tagziria, H., and Thomas D.J., Measurement and calculation of the emission anisotropy of an X1 ^{252}Cf neutron source, Radiat. Prot. Dosim. 126(1-4) (2007) 78-82.
- [8] Roberts N.J., Jones L.N., Wang Z., Liu Y., Wang Q., Chen X., Luo H., Rong C., Králik M., Park H., Choi K.O., Pereira W.W., da Fonseca E.S., Cassette P., Dewey M.S., Moiseev N.N., and Kharitonov I.A., International key comparison of measurements of neutron source emission rate (1999-2005) – CCRI(III)-K9. AmBe, Metrologia Tech. Suppl. 06018, 48 (2011) 35pp.
- [9] Hsu, H.-H. and Chen, J., Moderation of neutron spectra, Los Alamos National Laboratory report LA-UR-97-0749.
- [10] Pelowitz, D.B.(Editor), MCNPX User's Manual, Version 2.7.0 Los Alamos National Laboratory report, LA-CP-11-00438 (2011).
- [11] Pelowitz, D.B.(Editor), MCNPX 2.7.0 Extensions, Los Alamos National Laboratory report, LA-UR-11-02295 (2011).
- [12] HO Menlove, Description and operation manual for the active well coincidence counter, Los Alamos Scientific Laboratory report LA-7823-M, (1979).
- [13] HO Menlove and JE Swansen, A high-performance neutron time correlation counter, Nucl. Technol. 71(1985)498-505
- [14] Croft, S. and Chard, P.M.J., Neutronic characterization of plutonium oxide reference samples at Harwell, Proc. 15th Annual ESARDA Symp. on Safeguards and Nuclear Material Management, Rome, Italy, 11-13 May 1993. Report ESARDA 26 EUR 15214 EN CEC, Luxembourg, (1993)511-519.
- [15] Eckert & Ziegler, available at <http://www.ezag.com> (accessed on April 4th, 2017).
- [16] Frontier Technology Corporation, available at <http://www.frontier-cf252.com> (accessed on April 4th, 2017).
- [17] QSA Global Inc., available at <http://www.qsa-global.com/californium-252/> (accessed on April 4th, 2017).